J Nanostruct 16(3): 4085-4095, Summer 2026

RESEARCH PAPER

# Structural Property Correlation in PVA/$Al_2O_3$ Nanocomposites: Insights into Optical Band Gap Tuning

*Ibtisam Hamzah Radhi Abdul Hussein* *, *Zaid A. Hasan*

*Department of Physics, College of Education for Pure Sciences, University of Babylon, Iraq*

ARTICLE INFO

***Article History:***
*Received 07 March 2026*
*Accepted 22 June 2026*
*Published 01 July 2026*

***Keywords:***
*Aluminum oxide nanoparticles*
*Optical band gap tuning*
*Photoluminescence*
*Polymer nanocomposites*
*Structural ordering*

ABSTRACT

This study reports the fabrication and comprehensive characterization of polyvinyl alcohol (PVA)-based nanocomposite films reinforced with aluminum oxide ($Al_2O_3$) nanoparticlesvia a solution casting method. The influence of nanoparticle loading (0–6 wt.%) on the structural, morphological, and optical properties of the nanocomposites was systematically. investigated. X-ray diffraction (XRD) analysis confirmed the semi-crystalline nature of pure PVA, while enhanced crystallinity was observed upon incorporation of $Al_2O_3$ nanoparticles due to improved interfacial interactions. Fourier transform infrared spectroscopy (FTIR) revealedthe formation of hydrogen bonding between PVA chains and $Al_2O_3$ nanoparticles. Morphological analysis using FESEM demonstrated uniform nanoparticle dispersion at. lower concentrations, with partial agglomeration at higher loading levels. Optical studies indicated a significant reduction in the optical band gap from 4.8 eV to 4.1eV with increasing nanoparticle concentration, attributed to the formation of localized defect states and structural rearrangements within the polymer matrix. Photoluminescence (PL) spectra exhibited a dominant blue emission centered at ~485 nm, associated with. oxygen vacancy-related defect states in $Al_2O_3$ nanoparticles. The results demonstrate a strong structure–property correlation, highlighting the effectiveness of $Al_2O_3$ incorporation in tailoring the optical and structural properties of PVA. These findings suggest that the developed nanocomposites are promising candidates. for advanced optoelectronic and dielectric applications.

**How to cite this article**
*Abdul Hussein I., Hasan Z. Structural Property Correlation in PVA/$Al_2O_3$ Nanocomposites: Insights into Optical Band Gap Tuning. J Nanostruct, 2026; 16(3):4085-4095. DOI: 10.22052/JNS.2026.03.092*

## INTRODUCTION

Inelastic deformation of polymers generally occurs through chain sliding and flow, and on the nanometric scale, polymers are more likely to diffuse through the nanoparticle either with sliding or rearrangement. The considerable ability of one additive to enhance the properties of a polymer matrix can be explained on the basis of the large surface area of that compound [1-5]. Extrusion and solvent-casting are established techniques for the preparation of nanocomposites. The rest time to evaporate the solvent can be reduced by employing a volatile solvent or by pre-melting the polymer. However, when the viscosity of the matrix increases after a certain time, the rotational motion of the iron oxide-particle-filled composite is affected and the melt process becomes difficult. In a hybrid system, iron oxide is firstly grafted with

* *Corresponding Author Email: Ibtisam.alhussin.pure406@gmail.com*

vinyl-functionalized silane to provide a coupling agent between polyvinyl acetate (PVA) matrix and insoluble iron oxide in alcohol. Polyvinyl acetate is converted to polyvinyl alcohol (PVA) suitable for melt processing [6-13].

Polyvinyl alcohol (PVA) is a water-soluble, non-toxic, biodegradable, synthetic polymer with a simple structure, excellent biocompatibility, and high economic efficiency. It also exhibits unique properties such as flexibility, film formation, strong adhesion, gas barrier, and antibacterial ability. PVA is widely used in the electronics industry, textiles, papermaking, agriculture, medicine and biomedical applications, sealants and adhesives, coatings, food packaging, and materials such as lubricants, emulsifiers, and thickeners. Polyvinyl alcohol is produced by hydrolysis and represents the largest group of vinyl polymers commercially produced worldwide. Depending on the extent of hydrolysis, polyvinyl alcohol is classified into several grades [14-17].

Alumina nanoparticles, $Al_2O_3$ NPs or gamma-$Al_2O_3$ NPs, belong to the area of nanotechnology which is currently one of the most actively developed fields of research and application. They are solid materials built from two or more constituents, among which Al and O atoms are present. Not only are they one of the most popular nanoparticle systems regarded in scientific literature, but they also exhibit unique properties that arise as a result of their extremely small sizes and high specific surface area. They can show very high surface reactivity; therefore, functionalization of the surface is a common practice. Zeta potential measurements indicate the possibility of particle disaggregation in a liquid. $Al_2O_3$ NPs effectively facilitate catalytic reactions in environments that range from high vacuum to the presence of aggressive chemicals used in the petrochemical industry, which is an important constraint in chemical synthesis. $Al_2O_3$ NPs have a wide range of applications. They are used as catalysts and catalyst supports for various reactions, for instance in exhaust gas treatment in the automotive industry, synthesis of carbon black, or as catalysts for fast conversion of aliphatic alcohols into hydrocarbons. They can either act as carriers of active metal nanoparticles or as active catalysts in themselves. Applications in heterogeneous catalysis for energy conversion present another noteworthy opportunity. $Al_2O_3$ NPs are often applied as additives in a wide range of electronic components and coatings to enhance their physical and chemical properties, for instance as dielectric materials, thermal management materials, and reliability enhancement materials. When applied as dielectric materials in electronic components, the influence of $Al_2O_3$ NPs has been shown to improve dielectric properties as well as thermal conductivity, and thus reliability. $Al_2O_3$ NPs can also serve as antimicrobials, drug carriers, bone repair materials, and antireflective coatings [18]. Alumina exhibits excellent dielectric properties and retains reliable performance under extreme conditions.

As a result, $Al_2O_3$ nanoparticles are increasingly exploited in electronic components and substrates to enhance device performance and reliability. The use of $Al_2O_3$ as a dielectric or gate insulator improves the performance of Si-based field-impact transistors, metal-oxide-semiconductor capacitors, complementary metal-oxide-semiconductor (CMOS) technology [19], and these dielectric films can be easily integrated with organic semiconductors such as pentacene, and naphthalene diimide. Furthermore, the use of $Al_2O_3$ nanoparticles as a bulking agent in organic semiconductor formulations allows the optimization of the dielectric constant and charge transport, improving the electrical performance of devices based on organic-inorganic mixtures or polymer systems [20]. Additionally, $Al_2O_3$ films enable the integration of dielectrics with organic semiconductors in organic light-emitting diodes; such $Al_2O_3$ films can be deposited on different substrate materials and semiconductors containing metals, thus facilitating the production of hybrid organic-photonic devices [21].

## MATERIALS AND METHODS

### *Materials*

Polyvinyl alcohol (average molecular weight ~85,000 g/mol) and $Al_2O_3$ nanoparticles were used as received.

### *Film Preparation*

a) PVA dissolved by distilled water under magnetic stirring at 75°C even complete, b) dissolution. $Al_2O_3$ nanoparticles were ultrasonically dispersed for 30 minutes to minimize c) agglomeration the nanoparticle suspension was gradually introduced with PVA, d) sol at 2, 4, 6 wt.% concentrations.

The mix was stirred for 1 hour and flow in Petri

dishes. Films were dried at room temperature for 24 hours. The average thickness was approximately 105 µm as it is clear in Table 1.

*Statistical Analysis*

All measurements were conducted in triplicate. Reported values represent mean ± standard deviation. Statistical significance was evaluated using one-way ANOVA ($p < 0.05$).

## RESULTS AND DISCUSSION

*Structural Analysis (XRD)*

Pure PVA appear a wide diffraction at (2θ ≈ 20°), confirming its semi-crystalline nature. Upon $Al_2O_3$ incorporation, additional diffraction peaks corresponding to orthorhombic $Al_2O_3$ were observed.

$$D = \frac{0.9\,\lambda}{\beta \cos\theta} \quad (1)$$

Where β is the full width of the observed diffraction at half of the maximum intensity measured in radians, θ is the Bragg's angle and λ is X-ray wavelength, D is crystalline size measured in nm.

The calculated crystallite size was found to be reducing from 58.78nm to 36.1 nm with increasing nanoparticle loading, indicating nucleation-induced structural ordering within the polymer matrix as shown in the Table 3.

The XRD patterns were used to determine the crystallographic structure of PVA polymer and its nanocomposite films. The nanocomposites had varying ratios (2, 4, and 6 wt.%) of $Al_2O_3$ NPs. The purpose of this analysis was to identify the structure of the polymer nanocomposites at room temperature, as depicted in Fig. 1a. The figure shows that the PVA displays broad diffraction peaks at 2θ = 20.086° (strong), which indicate its amorphous nature [24]. The nanocomposites with high $Al_2O_3$ loading (6 wt.%) showed pronounced XRD peaks at 11.732°, 19.360°, 25.535°, 34.978°, 37.521°, 43.151°, 52.413°,57.498°, 66.578°, 67.850° corresponding to the miller indices of (020), (110), (130), (112), (112) (151), (242),

Table 1. Weight percentages for nanocomposites (PVA-$Al_2O_3$).

| PVA (gm) | $Al_2O_3$(gm) |
|---|---|
| 1 | 0 |
| 0.98 | 0.02 |
| 0.96 | 0.04 |
| 0.94 | 0.06 |

Table 2. Comparison of Optical Band Gap with Previous Studies.

| System | Band Gap (eV) | Method | References |
|---|---|---|---|
| PVA / ZnO | 5.4- 3.3 | Solvent casting | [22] |
| PVA / $TiO_2$ | 5.5 – 4.46 | Solution method | [23] |
| PVA/$Al_2O_3$ (This work) | 4.8 – 4.1 | Solvent casting | Present study |

Table 3. Structural, Energy gap of the synthesized $Al_2O_3$ NPs.

| Concentration | Peak position 2θ | FWHM | $D_{XRD}$ /nm | $D_{FESEM}$/ nm | Eg eV |
|---|---|---|---|---|---|
| 0 | 20.70 | 0.425 | 34.88 | 58.78 | 4.8 |
| 0.02 | 17.90 | 0.567 | 25.66 | 46.20 | 4.7 |
| 0.04 | 17.72 | 0.584 | 24.91 | 41.28 | 4.4 |
| 0.06 | 17.17 | 0.597 | 24.27 | 36.10 | 4.1 |

(332), (441), and (114)). The peaks were indexed with Powder X software and contrast with the standard JCPDS card file No. 37-1463 (space group number 63) which the formation of $Al_2O_3$in Orthorhombic crystal system (a = 6.618 Å, b = 11.944A°, c = 5.724 Å°) [25]. From the Fig. 1 down of the nanocomposites, it is recognized that $Al_2O_3$ NPs at (6 wt.%) take effect on the structural characteristics of PVA.

*Fourier Transformation Infrared Ray Spectroscopy (FTIR)*

The spectrometer (FTIR) is used in the analysis of a board range of materials such as thin films and powders. It provides information both for mixture composition and polymer-polymer reactions using those vibrational modes attributed to free and hydrogen hydroxyl and carbonyl groups. FTIR spectra of PVA-$Al_2O_3$ nanocomposites with different doped ratios of $Al_2O_3$ nanoparticles are Record measurements in the spectrum range 400 – 4000 $cm^{-1}$. FTIR spectroscopy of PVA-$Al_2O_3$ nanocomposite films are shown in Fig. 2a. This film exhibits peaks at 3417.86, 2931.80, 1741.72, 1637.56,1620.21, 1544.98, 1512.19, 613.36, 420.48 $cm^{-1}$ It is assigned to links O-H, C-H, C=O

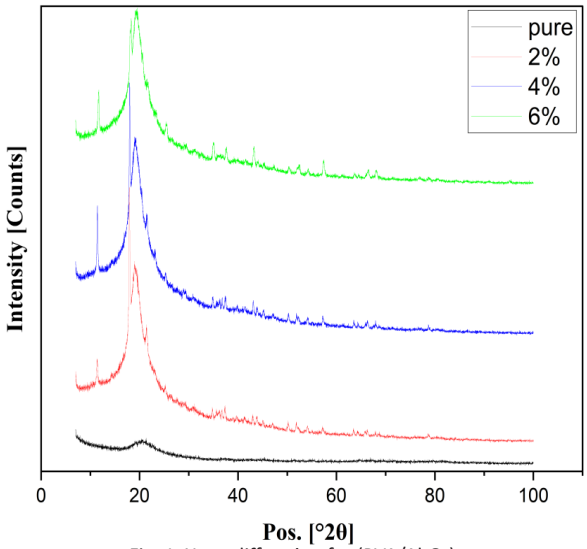


Fig. 1. X-ray diffraction for (PVA/$Al_2O_3$).

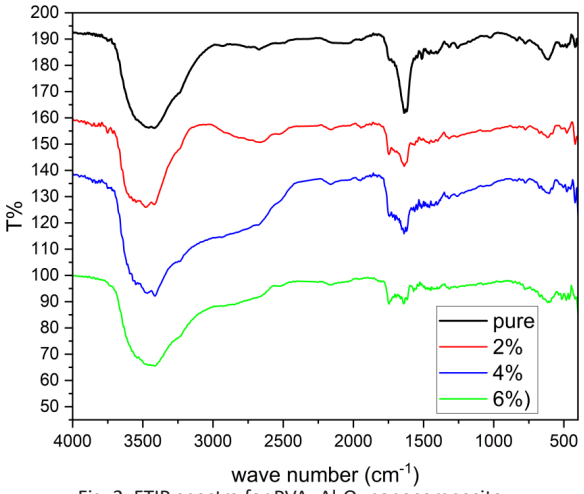


Fig. 2. FTIR spectra for PVA- $Al_2O_3$ nanocomposite.

stretching's, bending of $CH_2$, C-O stretching, $CH_2$ rocking, $CH_2$ stretching and O-H wagging, respectively [24]. The O-H stretching, has the most characteristic alcohol bonds and is within the spectrum 3400 $cm^{-1}$. The band returns to the band around 1415 $cm^{-1}$ to the curvature the $CH_3$ bond and the bands around it 2900 $cm^{-1}$ correspond to $CH_2$ asymmetric stretching. The range at 916.15 $cm^{-1}$ is due to the syntenic structure and is caused by the $CH_2$ vibration. Referred to PVA crystal and around 1750 $cm^{-1}$ of the carbonyl that results from the absorption of the remainder of the acetate during the period of manufacture of PVA by the hydrolysis of polyvinyl acetate. The band at 1330 $cm^{-1}$ was assigned to the combination frequency of CH+OH. The peaks at 1649 $cm^{-1}$ have been assigned to the C=C stretching mode. The Fig. 2a shows the FTIR spectra of PVA while Figs. 2b-d show the FTIR spectra of PVA-$Al_2O_3$ nanocomposites Changing the FTIR spectrum in range 1600 to 3400 $cm^{-1}$ shows that the product of the polymer chains corresponds to the O-H bond stretching, and the C-H bond stretching [26]. By the addition of $Al_2O_3$ nanoparticles to polymer blends, two significant changes are observed. There are slight changes in the intensity of absorption and in the vibrational

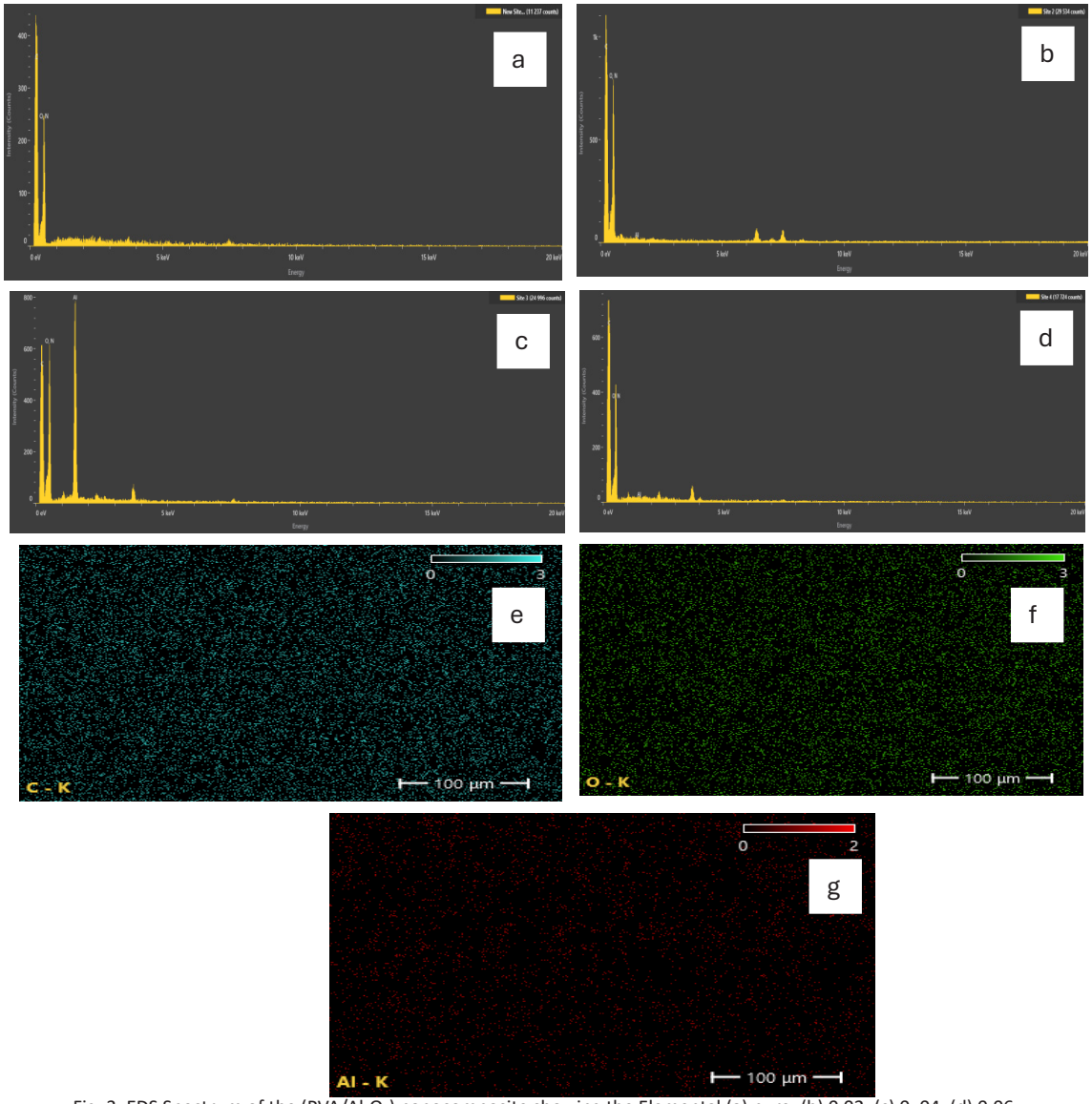


Fig. 3. EDS Spectrum of the (PVA/$Al_2O_3$) nanocomposite showing the Elemental (a) pure, (b) 0.02, (c) 0. 04, (d) 0.06.

bands, this indicates decoupling between the corresponding vibrations due to interaction between $Al_2O_3$ nanoparticles and PVA [27].

*Energy-Dispersive Spectrometer (EDS).*

Energy Dispersive X-ray Spectroscopy (EDS), carried out along SEM, because used to analyze the basic composition of the synthesized nanocomposites. In the EDS spectrum of PVA/$Al_2O_3$ (Fig. 3), the characteristic peaks of carbon (C) and oxygen (O) are attributed to the PVA polymer matrix, where carbon originates from the polymer backbone and oxygen arises from both the polymer's functional groups (–OH and C=O) and the metal oxide nanoparticles. The clear signals of Al confirm the successful incorporation of $Al_2O_3$ within the polymeric structure [28]. And (EDX) confirmed the presence of Al and O elements without contamination.

*Field Emission Scanning Electron Microscope (FESEM)*

The surface morphology of PVA/$Al_2O_3$ nanocomposites with varying concentrations. is shown in Fig. 4 using Scanning Electron Microscopy (SEM). Fig. 4a refers to the SEM micrograph of a pure PVA polymer, illustrating its smooth and homogeneous surface morphology, without

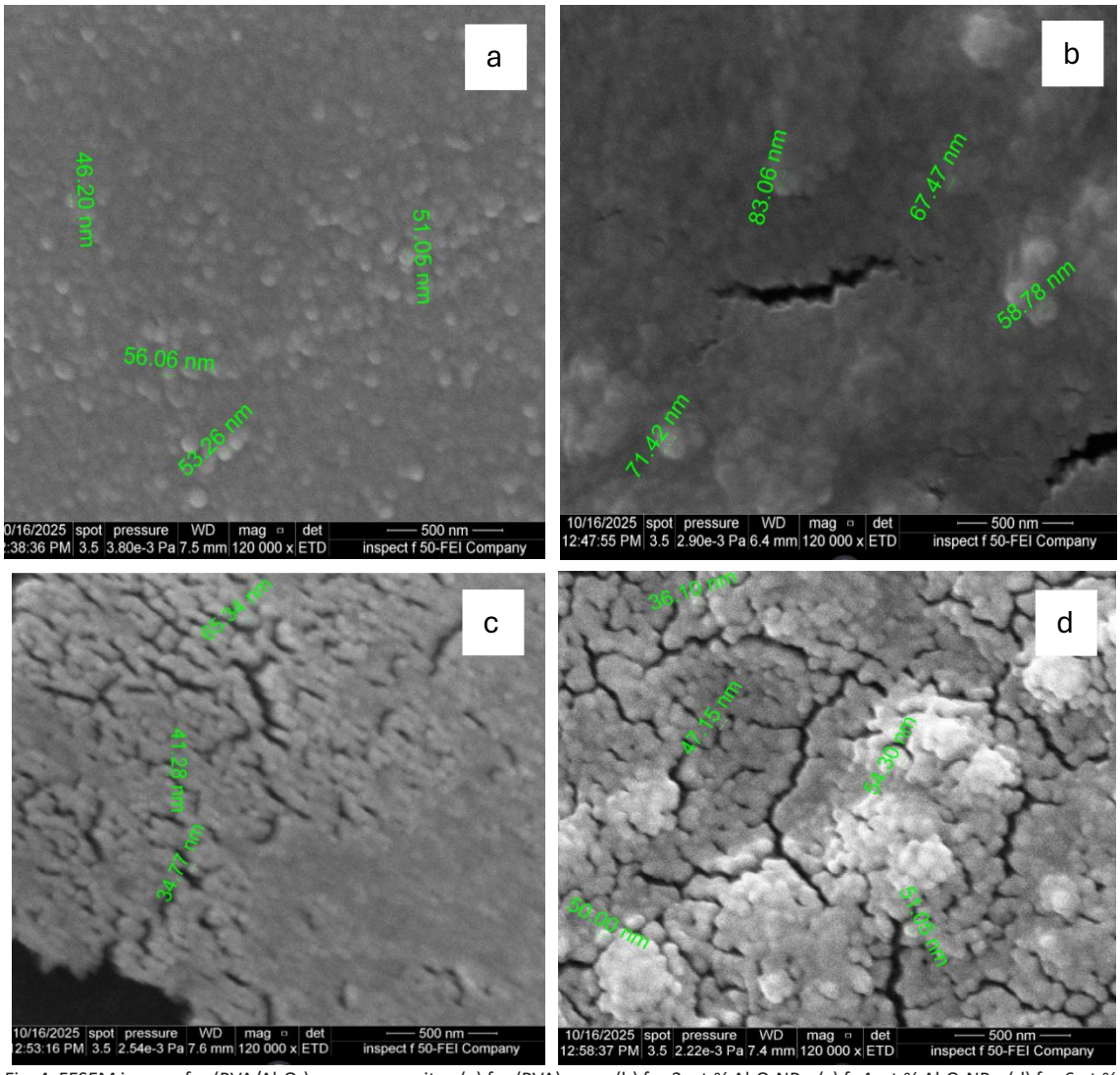


Fig. 4. FESEM images for (PVA/$Al_2O_3$) nanocomposites:(a) for (PVA) pure, (b) for 2 wt.% $Al_2O_3$NPs, (c) fr 4 wt.% $Al_2O_3$NPs, (d) for 6wt.% $Al_2O_3$NPs.

the presence of nanoparticles. This baseline morphology serves as a reference for comparing the changes induced by the incorporation of metal oxide nanoparticles in subsequent nanocomposite samples [29].

By increasing concentration of $Al_2O_3$ nanoparticles in the PVA matrix, the SEM images demonstrate a transition from a relatively uniform dispersion at lower concentrations (2–4 wt.%) to more aggregated structures and rougher surfaces at higher loading (6 wt.%). This morphological evolution is attributed to the increased particle–particle interactions, which may enhance or hinder the electrical and sensing properties depending on the extent of agglomeration [30].

At 6 wt.% loading of $Al_2O_3$ nanoparticles, the SEM image expose a relatively homogeneous distribution of nanoparticles throughout the polymer matrix with moderate surface roughness. The image shows the beginning of particle aggregation, but without severe agglomeration, indicating a partially balanced dispersion. This concentration offers an optimized morphology where the nanoparticles are sufficiently abundant to provide enhanced interfacial interaction and active sites. Such morphology is favorable for improving the electrical and biosensing properties of the nanocomposite due to effective charge transfer pathways and accessible surface area [31,32].

*Optical Properties*

*Uv- Vis and Band Gap*

The effect of varying concentrations of PVA

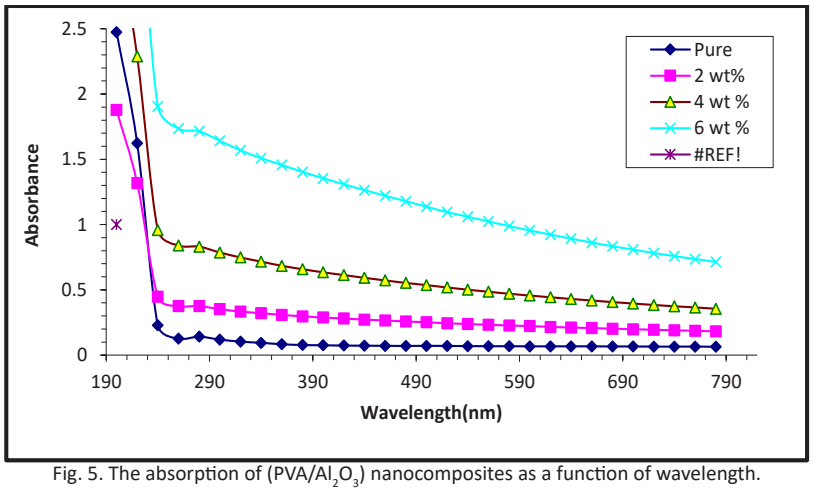


Fig. 5. The absorption of (PVA/$Al_2O_3$) nanocomposites as a function of wavelength.

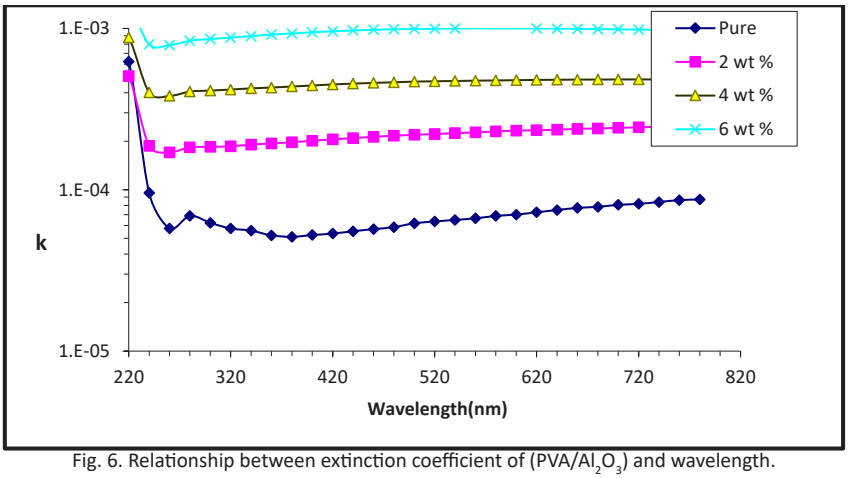


Fig. 6. Relationship between extinction coefficient of (PVA/$Al_2O_3$) and wavelength.

on the optical properties of $Al_2O_3$ nanoparticles (NPs) was systematically investigated using UV–Vis spectroscopy over the wavelength range of 190–790 nm at room temperature. As illustrated in Fig. 5, all samples exhibit a prominent absorption edge around 220 nm,which corresponds to the electronic transition from the valence band to the conduction band.

A noticeable decrease in absorbance intensity was observed with increasing PVA concentration, accompanied by a slight blue shift toward lower wavelengths in the UV region. This shift can be attributed to changes in the electronic structure of the nanoparticles, particularly variations in the band gap energy. Typically, a shift toward lower wavelengths indicates an increase in band gap energy; however, this behavior may also be.influenced by particle dispersion and interaction with the polymer matrix [33,34].

The extinction coefficient (k) was calculated using the Eq. 2:

$$k = \frac{\alpha\lambda}{4\pi} \quad (2)$$

where α is the absorbance and λ is the wavelength. The plot of extinction coefficient versus photon energy (Fig. 6) shows a linear region, which was extrapolated to determine the optical band gap. The results indicate that the optical parameters are strongly dependent on nanoparticle concentration, consistent with

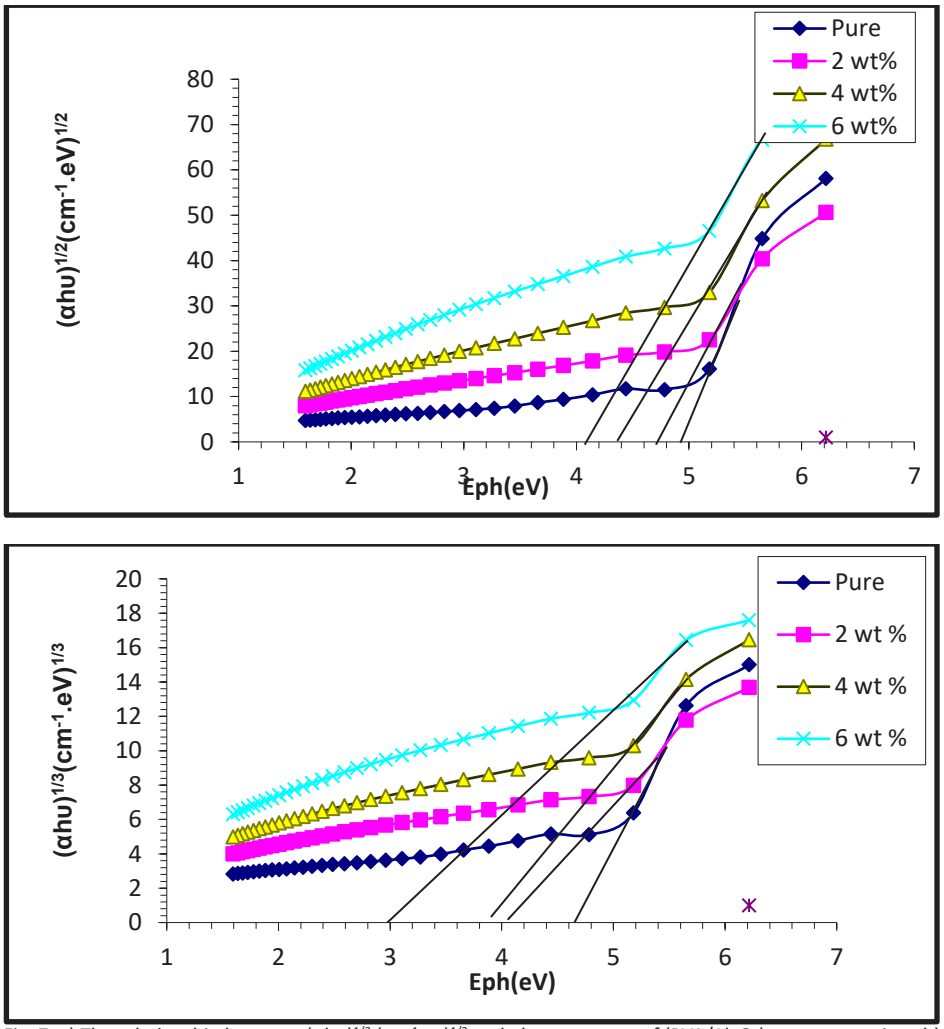


Fig. 7. a) The relationship between $(\alpha h\upsilon)^{1/2}$ $(cm^{-1}.ev)^{1/2}$ and photon energy of ($PVA/Al_2O_3$) nanocomposites, b) The relationship between $(\alpha h\upsilon)^{1/3}$ $(cm^{-1}.ev)^{1/3}$ and the photons energy of the ($PVA/Al_2O_3$) nanocomposites.

structural findings obtained from XRD and TEM analyses

From a physical perspective, increasing particle size generally leads to a reduction in bandgap energy due to decreased quantum confinement effects. As particle size increases, the number of atoms per particle also increases, enhancing electron–ion core interactions, which in turn reduces the energy separation between the valence and conduction bands

To further identify the nature of electronic transitions, the Mott–Davis model [35] was applied Eq. 3.

$$(\alpha\, hv)^{n} = A\left(hv - E_g\right) \quad (3)$$

where A is a constant, hu is the photon energy, and $E_g$ is the optical band gap. The exponent determines the type of transition. By analyzing the plots for different values of the best linear fit was obtained for indicating that the dominant transition in $Al_2O_3$ NPs is a direct allowed transition. Moreover, the optical band gap was found to decrease from 4.8 eV (pure PVA) to 4.1 eV at 6 wt.% $Al_2O_3$. This reduction can be explained by several factors: 1- Formation of localized defect states within the band structure, 2- Enhanced interfacial polarization between polymer and nanoparticles, 3- Structural rearrangements in the polymer matrix.

These factors introduce intermediate energy levels within the forbidden gap, facilitating electronic transitions at lower energies. The obtained band gap values are in good agreement with previously reported studies, confirming the reliability of the experimental approach and supporting the proposed physical interpretation [33-38].

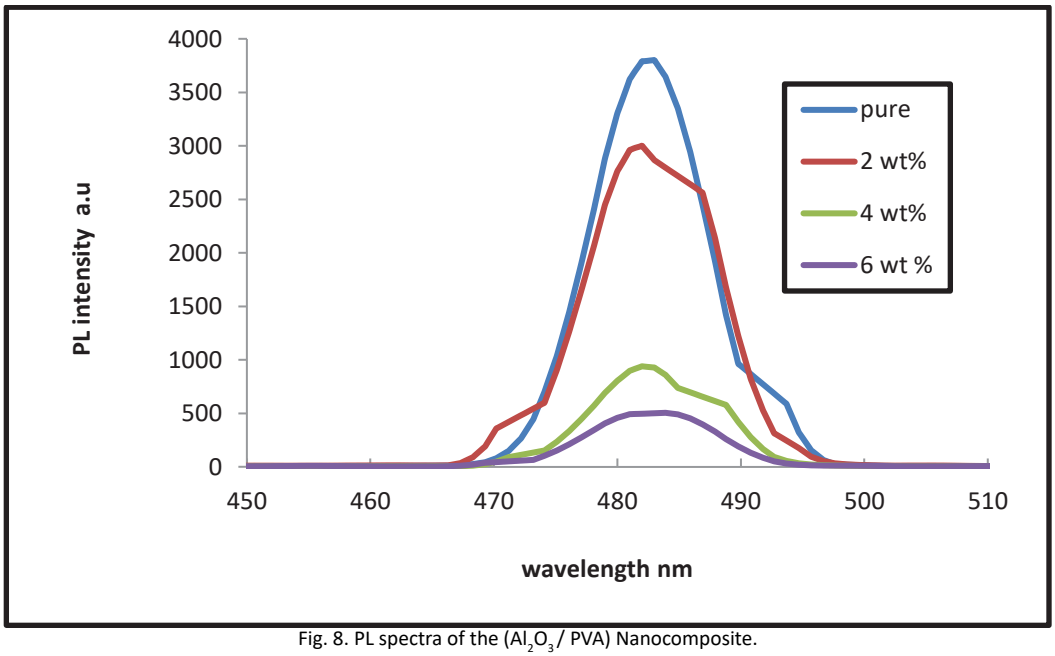


Fig. 8. PL spectra of the ($Al_2O_3$/ PVA) Nanocomposite.

Table 4. The energy gap for the allowed and forbidden indirect transition for (PVA/$Al_2O_3$) nanocomposites.

| $Al_2O_3$ NPs wt.% | The optical energy gap of the indirect transition (eV) | |
|---|---|---|
| | Allowed | Forbidden |
| 0 | 4.8 | 4.6 |
| 2 | 4.7 | 4.1 |
| 4 | 4.4 | 3.8 |
| 6 | 4.1 | 3 |

*Photoluminescence study*

PL spectra showed a prominent emission peak centered at ~485 nm in the blue region. This emission an attributed to defect-related states, particularly oxygen vacancies in $Al_2O_3$ nanoparticles and interfacial trap states within the nanocomposite structure. The emission intensity varied with nanoparticle concentration, indicating modified recombination dynamics and defect density as shown in Fig. 8 [39- 42].

## CONCLUSION

$Al_2O_3$-reinforced PVA nanocomposites were successfully fabricated using a solvent casting technique. Structural analysis demonstrated enhanced crystallinity with increasing nanoparticle loading. Optical measurements revealed tunable band gap behavior and defect-mediated blue emission. The results confirm that controlled incorporation of $Al_2O_3$ nanoparticles effectively modifies the structural ordering and optical properties of PVA films, highlighting their potential for dielectric layers, optical coatings, and optoelectronic applications.

## CONFLICT OF INTEREST

The authors declare that there is no conflict of interests regarding the publication of this manuscript.

## REFERENCES


1. Kang D, Tong S, Yu X, Ge M. Template-free synthesis of 3D hierarchical amorphous aluminum oxide microspheres with broccoli-like structure and their application in fluoride removal. RSC Advances. 2015;5(25):19159-19165.
2. Atrak K, Ramazani A, Taghavi Fardood S. Green synthesis of amorphous and gamma aluminum oxide nanoparticles by tragacanth gel and comparison of their photocatalytic activity for the degradation of organic dyes. Journal of Materials Science: Materials in Electronics. 2018;29(10):8347-8353.
3. Mohammed AA, Khodair ZT, Khadom AA. Preparation and investigation of the structural properties of α-Al2O3 nanoparticles using the sol-gel method. Chemical Data Collections. 2020;29:100531.
4. Rutkowska I, Marchewka J, Jeleń P, Odziomek M, Korpyś M, Paczkowska J, et al. Chemical and Structural Characterization of Amorphous and Crystalline Alumina Obtained by Alternative Sol–Gel Preparation Routes. Materials. 2021;14(7):1761.
5. Abdulridha GR, Hasan ZA. Study the Effect Doping (Al2O3) Nanoparticles on Optical Properties for PVA Polymer. Neuroquantology. 2022;20(3):231-236.
6. Hussein Kamil M, Zaid AH, Khalid A-A. Improving the Structural and Morphological Characteristic of Carboxymethyl cellulose (CMC) Via Additive ZnSe Nanoparticle. International Journal of Computational and Experimental Science and Engineering. 2025;11(1).
7. Tang X, Alavi S. Recent advances in starch, polyvinyl alcohol based polymer blends, nanocomposites and their biodegradability. Carbohydr Polym. 2011;85(1):7-16.
8. Baker MI, Walsh SP, Schwartz Z, Boyan BD. A review of polyvinyl alcohol and its uses in cartilage and orthopedic applications. Journal of Biomedical Materials Research Part B: Applied Biomaterials. 2012;100B(5):1451-1457.
9. Geen, Burnard, (30 July 1882–16 March 1966), practice, Consulting and Chartered Civil Engineer, since 1910. Who Was Who: Oxford University Press; 2007.
10. Effects of Composition, Processing, and Structure on Properties of Engineering Plastics. Characterization and Failure Analysis of Plastics: ASM International; 2003. p. 28-48. http://dx.doi.org/10.31399/asm.tb.cfap.t69780028
11. Xu X, Zhao J, Wang M, Wang L, Yang J. 3D Printed Polyvinyl Alcohol Tablets with Multiple Release Profiles. Sci Rep. 2019;9(1).
12. Blum MM, Ovaert TC. A novel polyvinyl alcohol hydrogel functionalized with organic boundary lubricant for use as low-friction cartilage substitute: Synthesis, physical/chemical, mechanical, and friction characterization. Journal of Biomedical Materials Research Part B: Applied Biomaterials. 2012;100B(7):1755-1763.
13. Chaouat M, Le Visage C, Baille WE, Escoubet B, Chaubet F, Mateescu MA, et al. A Novel Cross-linked Poly(vinyl alcohol) (PVA) for Vascular Grafts. Adv Funct Mater. 2008;18(19):2855-2861.
14. Kawai F, Hu X. Biochemistry of microbial polyvinyl alcohol degradation. Applied Microbiology and Biotechnology. 2009;84(2):227-237.
15. Byrne D, Boeije G, Croft I, Hüttmann G, Luijkx G, Meier F, et al. Biodegradability of Polyvinyl Alcohol Based Film Used for Liquid Detergent Capsules. Tenside Surfactants Detergents. 2021;58(2):88-96.
16. DeMerlis CC, Schoneker DR. Review of the oral toxicity of polyvinyl alcohol (PVA). Food and Chemical Toxicology. 2003;41(3):319-326.
17. Adelnia H, Ensandoost R, Shebbrin Moonshi S, Gavgani JN, Vasafi EI, Ta HT. Freeze/thawed polyvinyl alcohol hydrogels: Present, past and future. Eur Polym J. 2022;164:110974.
18. Radziun E, Dudkiewicz Wilczyńska J, Książek I, Nowak K, Anuszewska EL, Kunicki A, et al. Assessment of the cytotoxicity of aluminium oxide nanoparticles on selected mammalian cells. Toxicol In Vitro. 2011;25(8):1694-1700.
19. Lorenz M, Ramachandra Rao MS, Venkatesan T, Fortunato E, Barquinha P, Branquinho R, et al. The 2016 oxide electronic materials and oxide interfaces roadmap. J Phys D: Appl Phys. 2016;49(43):433001.
20. Siddiq MA. Synthesis of $Alq_3$ by a facile co-precipitation approach and study the impact of CNTs support on its microstructure and electronic characteristics for photodiode development. Materials Research Express. 2023;10(6):066301.
21. Weis M. Organic Semiconducting Polymers in Photonic Devices: From Fundamental Properties to Emerging Applications. Applied Sciences. 2025;15(7):4028.
22. Dejen KD, Zereffa EA, Murthy HCA, Merga A. Synthesis of ZnO and ZnO/PVA nanocomposite using aqueous Moringa Oleifeira leaf extract template: antibacterial and electrochemical activities. Reviews On Advanced Materials Science. 2020;59(1):464-476.
23. Venugopal R, Srinivas CH. Conductivity and Bandgap Engineering in PVA-$TiO_2$ Nanocomposites for Optoelectronic Device Applications. Journal of Physics: Conference Series.

2024;2778(1):012009.
24. Suki FMM, Azahari NA, Othman N, Ismail H, Sasidharan S. Biodegradation Studies of Attapulgite Clay Filled Polyvinyl Alcohol/Modified Corn Starch Blend Films: Microbial and Enzymatic. Advanced Materials Research. 2013;747:668-672.
25. Lee H, Chung WJ. $Eu^{2+}$-doped oxyfluoride glass-ceramic with nepheline as an efficient 400 nm UV-LED color converter. J Am Ceram Soc. 2021;104(8):4024-4032.
26. Ali Abed E. The Effect of the Poly Vinyl Chloride (PVC) Addition on Surface Hardness and Impact Strength Properties of Heat-Cured Acrylic Resin Denture Base Material. Journal of University of Anbar for Pure Science. 2010;4(3):50-53.
27. Wang S-N, Zhang F-D, Huang A-M, Zhou Q. Distinction of four Dalbergia species by FTIR, 2nd derivative IR, and 2D-IR spectroscopy of their ethanol-benzene extractives. Holzforschung. 2015;70(6):503-510.
28. Mohamed HFM, Abdel-Hady EE, Abdel-Moneim MMY, Bakr MAM, Soliman MAM, Shehata MGH, et al. Effect of Al2O3 on Nanostructure and Ion Transport Properties of PVA/PEG/SSA Polymer Electrolyte Membrane. Polymers. 2022;14(19):4029.
29. Abhilash MR, Akshatha G, Srikantaswamy S. Photocatalytic dye degradation and biological activities of the $Fe_2O_3/Cu_2O$ nanocomposite. RSC Advances. 2019;9(15):8557-8568.
30. Ramesan MT, George A, Jayakrishnan P, Kalaprasad G. Role of pumice particles in the thermal, electrical and mechanical properties of poly(vinyl alcohol)/poly(vinyl pyrrolidone) composites. J Therm Anal Calorim. 2016;126(2):511-519.
31. El Rahman A, Metwally HS, Sabry N, Mohammed MI. Gamma-ray shielding effectiveness, optical, mechanical, dielectric properties of nanofiller-reinforced PVA/PVP polymeric blend nanocomposites. Sci Rep. 2024;14(1).
32. Ul-Hamid A. Contrast Formation in the SEM. A Beginners' Guide to Scanning Electron Microscopy: Springer International Publishing; 2018. p. 77-128. http://dx.doi.org/10.1007/978-3-319-98482-7_3
33. Alnahari H, Al-Sharabi A, Al-Hammadi AH, Al-Odayni A-B, Alnehia A. Synthesis of glycine-mediated CuO–$Fe_2O_3$–MgO nanocomposites: Structural, optical, and antibacterial properties. Composites and Advanced Materials. 2023;32.
34. Babu KS, Reddy AR, Reddy KV, Mallika AN. High thermal annealing effect on structural and optical properties of ZnO–$SiO_2$ nanocomposite. Mater Sci Semicond Process. 2014;27:643-648.
35. Babu KS, Reddy AR, Reddy KV. Controlling the size and optical properties of ZnO nanoparticles by capping with SiO2. Mater Res Bull. 2014;49:537-543.
36. Davis EA, Mott NF. Conduction in non-crystalline systems V. Conductivity, optical absorption and photoconductivity in amorphous semiconductors. Philos Mag. 1970;22(179):0903-0922.
37. Mishra KC, Johnson KH, DeBoer BG, Berkowitz JK, Olsen J, Dale EA. First principles investigation of electronic structure and associated properties of zinc orthosilicate phosphors. J Lumin. 1991;47(5):197-206.
38. Lee CS, Matori KA, Ab Aziz SH, Mohamed Kamari H, Ismail I, Mohd Zaid MH. Influence of zinc oxide on the physical, structural and optical band gap of zinc silicate glass system from waste rice husk ash. Optik. 2017;136:129-135.
39. Al-Hada N, Saion E, Talib Z, Shaari A. The Impact of Polyvinylpyrrolidone on Properties of Cadmium Oxide Semiconductor Nanoparticles Manufactured by Heat Treatment Technique. Polymers. 2016;8(4):113.
40. Fu Z, Yang B, Li L, Dong W, Jia C, Wu W. An intense ultraviolet photoluminescence in sol gel ZnO $SiO_2$ nanocomposites. J Phys: Condens Matter. 2003;15(17):2867-2873.
41. Jung KY, Han KH. Densification and Photoluminescence Improvement of $Y_2O_3$ Phosphor Particles Prepared by Spray Pyrolysis. Electrochem Solid-State Lett. 2005;8(2):H17.
42. Shu Shunpeng, Tao Chunxian, Ruan Jun, Hong Ruijin, Zhang Dawei. Measurement of Conversion Efficiency of Ultraviolet Down-Conversion Light-Emitting Thin Films. Acta Optica Sinica. 2015;35(10):1031001.